

PORE-PRESSURE RESPONSE DUE TO PENETRATION THROUGH LAYERED MEDIA

DEREK ELSWORTH

*Department of Mineral Engineering, Pennsylvania State University, 104 Mineral Sciences Building,
University Park, PA 16802, U.S.A.*

SUMMARY

A solution is developed for a point dislocation traversing a slab of saturated porous material under prescribed upper and lower hydraulic boundary conditions as an analogue to penetration in a layer of finite thickness. Pressure response is conditioned by geometrical parameters and those of dimensionless penetration rate U_D , dimensionless time following penetration initiation t_D , and dimensionless time following penetration arrest t'_D . The extended set of dimensionless parameters controlling the response makes parameter determination problematic and questionably non-unique. Pressure response in the proximity of a lower permeable or impermeable boundary is indistinguishable from the homogeneous case for coefficients of consolidation c in excess of $2 \text{ cm}^2/\text{s}$. Below this threshold, penetration-generated pore pressures are visibly modified in the presence of a discrete boundary. *In situ* parameters inferred directly from pressure magnitudes, without due consideration for the influence of layering, may therefore be in considerable error. In the hydraulically visible range, the influence of layering on the generated tip pressures is apparent at a separation of the order of 1.5 cm for standard penetration. Although absolute pressure magnitudes are strongly modified in the presence of boundaries, dissipation rates remain relatively unaffected and are consistent with those recorded in the absence of boundaries. The monitoring of dissipation rates, post-arrest, is suggested as the most reliable and accurate method of extricating parameters, *in situ*.

1. INTRODUCTION

Piezocoones have been successfully utilized in the determination of mechanical and hydraulic properties of soils, *in situ*.¹⁻⁴ Traditional methods of interpretation consider penetrometer advance or arrest to be conditioned by the homogeneous surrounding medium^{5,6} without consideration of layering or lensing that may considerably affect the generation and subsequent dissipation of pore pressures. If the undrained strain field surrounding the penetrometer is determined, the pore-pressure distributions may be recovered from knowledge of the pore-pressure coefficients.^{7,8} Alternatively, the analysis may be conducted using the concepts of deformation in a poro-elastic medium where pore-fluid pressures are conditioned by the induced deformation field.^{9,10} Green's functions are available to represent both static¹¹ and moving¹² volumetric dislocations in poro-elastic media where the medium is homogeneous. Despite the inability of a linear analysis to represent the finite strain conditions likely at the tip of an advancing penetrometer, comparison with field data yields satisfactory agreement for penetration in unconsolidated media,¹³ even when compared against approximate non-linear analyses.¹⁴ This second-order influence of non-linearity appears conditioned by the essentially linear and small strain response of the material comprising the intermediate and far field. The applicability of a linear model may therefore diminish as the zone of non-linear behaviour surrounding the penetrometer becomes progressively larger. Additional application of dislocation models to

may be made with τ , the discrete parameter of time integration. A moving co-ordinate system is selected for the primary dislocation that moves with the dislocation at a rate U in the negative x -direction. The position of a point located relative to the primary dislocation at co-ordinates (x, y, z) at current time t would have been $[x - U(t - \tau), y, z]$ at time τ . Substituting equation (3) and the co-ordinate transformation into equation (1) and integrating over time (τ) between the time of initiation of penetration (0) and current time (t) gives¹²

$$P_D R_D = \frac{2}{\sqrt{\pi}} \int_{R_D/t_D}^{\infty} \exp \left[U_D x_D - \eta^2 - \left(\frac{U_D R_D}{2\eta} \right)^2 \right] d\eta \quad (4)$$

where the substitution $\eta = R/2[c(t - \tau)]^{1/2}$ is used as a dummy variable of integration and quantities are non-dimensionalised with respect to penetrometer radius, r . Thus,

$$P_D = \frac{4(p - p^s) k}{Ur} \frac{1}{\mu} \quad (5)$$

$$U_D = \frac{Ur}{2c} \quad (6)$$

$$t_D = \frac{4ct}{r^2} \quad (7)$$

$$(x_D, y_D, z_D) = \frac{1}{r} (x, y, z) \quad (8)$$

with

$$R_D^2 = x_D^2 + y_D^2 + z_D^2 \quad (9)$$

where the terms may be referred to as dimensionless pressure P_D , dimensionless penetration rate U_D and dimensionless time t_D within the non-dimensional space (x_D, y_D, z_D) . Dimensionless pressure is chosen specifically such that

$$0.0 \leq P_D R_D \leq 1.0 \quad (10)$$

for a single moving dislocation.

2.2 Image dislocations

Image dislocations must be supplied to enforce the boundary conditions mandated by the layered geometry represented in Figure 1. Penetration is initiated within a layer of thickness b at a height s above the lower layer boundary. The separation between any location in the moving co-ordinate x and the layer base is represented by w and $w = (s + x) - Ut$. Since the analysis is uncoupled, the image dislocations may also be viewed as fluid sources or sinks depending on the required boundary condition. Since the primary dislocation is reflected through a static confining boundary, as illustrated in Figure 1, the image dislocations must move at an identical rate (U) with the direction controlled by the reflection sequence of the confining stratigraphic boundaries. The disposition of image dislocations about the primary dislocation is given in Figure 2(a), where the first reflection is in the upper boundary, and in Figure 2(b), where the first reflection is in the lower boundary. These figures illustrate the initial primary co-ordinate system (x, y, z) and its derivatives (x'_i, y'_i, z'_i) corresponding to time $t = 0$. Following the initiation of penetration, all local co-ordinate systems move at a rate U in the local negative x - or x'_i -direction as depicted in Figure 2. Penetration initiates in a layer of thickness b , at a height s above the layer base.

of images initiated following first reflection in the upper bounding layer [Figure 2(a)] as

$$x'_2 = -2(nb + s - Ut) - x, \quad n < 0 \quad (11a)$$

$$x'_1 = 2nb + x, \quad n \geq 0 \quad (11b)$$

A similar co-ordinate transformation may be applied to the sequence of images resulting from the first reflection in the lower bounding layer [Figure 2(b)] as

$$x'_1 = 2nb + x, \quad n < 0 \quad (12a)$$

$$x'_2 = -2(nb + s - Ut) - x, \quad n \geq 0 \quad (12b)$$

where the sense of the dislocation is controlled by the boundaries and

$$R_{D_i}^{\prime 2} = \frac{1}{r^2} [x_i^{\prime 2} + y_i^{\prime 2} + z_i^{\prime 2}] \quad (12c)$$

The relationships are symmetric despite the apparently antisymmetric appearance of equations (11) and (12).

This is true, not only with respect to the sequence of positive and negative source strengths with integer magnitude n , but also with respect to the relative orientations of global (x, y, z) and local (x'_i, y'_i, z'_i) co-ordinate systems.

Since all of the image co-ordinate systems move at a uniform velocity U in the local, negative x'_i -direction, a homogeneous expression is obtained by introducing, at the origin, a point dislocation at the rate $U\pi r^2$ per unit time. For the moving co-ordinate system, therefore, $V = U\pi r^2 d\tau$ and the integration is completed for relative co-ordinates

$$(x''_i, y''_i, z''_i) = [x'_i - U(t - \tau), y'_i, z'_i] \quad (13)$$

Substituting equations (11) and (12) into (13), rearranging in dimensionless form by dividing through by penetrometer radius, r , and substituting $\eta = R/2 [c(t - \tau)]^{1/2}$ yields, for equations (11b) and (12a),

$$x''_{D_1} = 2nb_D + x_D - \frac{U_D R_D^2}{2\eta^2}, \quad -\infty < n < \infty \quad (14a)$$

and for equations (11a) and (12b),

$$x''_{D_2} = -2(nb_D - s_D) + U_D t_D - x_D - \frac{U_D R_D^2}{2\eta^2}, \quad -\infty < n < \infty \quad (14b)$$

where

$$b_D = \frac{b}{r}; \quad s_D = \frac{s}{r} \quad (14c)$$

and

$$y''_{D_1} = y_D; \quad z''_{D_1} = z_D \quad (14d)$$

Accordingly, equation (2) may be restated in dimensionless form as

$$\xi_i = \frac{R_{D_i}^{\prime 2} r}{[c(t - \tau)]^{1/2}}; \quad R_{D_i}^{\prime 2} = x_{D_i}^{\prime 2} + y_{D_i}^{\prime 2} + z_{D_i}^{\prime 2} \quad (15)$$

where $(\bar{x}_D, \bar{y}_D, \bar{z}_D)$, and therefore, \bar{R}_D are co-ordinates relative to the arrested geometry. Substituting equations (20)–(22) into (17), with revised integration limits, yields

$$\begin{aligned}
 P_D \bar{R}_D = & \frac{\bar{R}_D}{R_{D1}''} \frac{2}{\sqrt{\pi}} \sum_{n=-\infty}^{\infty} ij^n \int_{R_D/t_D^{1/2}}^{R_D/(t_D-t_D')^{1/2}} \exp \left\{ -\eta^2 \left[1 + a_1 \frac{(a_1 + 2x_D)}{R_D^2} \right] - \left[\frac{U_D R_D}{2\eta} \right]^2 \right. \\
 & \left. + U_D(x_D + a_1) \right\} d\eta + \frac{\bar{R}_D}{R_{D2}''} \frac{2}{\sqrt{\pi}} \sum_{n=-\infty}^{\infty} ln^n \int_{R_D/t_D^{1/2}}^{R_D/(t_D-t_D')^{1/2}} \\
 & \exp \left\{ -\eta^2 \left[1 + a_2 \frac{(a_2 - 2x_D)}{R_D^2} \right] - \left[\frac{U_D R_D}{2\eta} \right]^2 - U_D(x_D - a_2) \right\} d\eta
 \end{aligned} \quad (23)$$

where a_1 and a_2 are as previously defined in equation (18).

2.4. Dimensionless parameters

The pre-arrest and post-arrest pressure distributions represented by equations (17) and (23), respectively, may be reduced to a minimum set of dimensionless parameters. Pre-arrest, the functional dependence is

$$P_D R_D = f \left(U_D R_D; \frac{x_D}{R_D}; \frac{t_D}{R_D^2}; \frac{s_D}{R_D}; \frac{b_D}{s_D} \right) \quad (24)$$

and post-arrest this is modified to

$$P_D \bar{R}_D = f \left[U_D \bar{R}_D; \frac{\bar{x}_D}{R_D}; \frac{(t_D - t_D')}{\bar{R}_D^2}; \frac{t_D'}{\bar{R}_D^2}; \frac{s_D}{R_D}; \frac{b_D}{s_D} \right] \quad (25)$$

where interest is retained in the local co-ordinate system relative to the arrested geometry.

The general form of the induced and concurrently dissipating pressure distribution around the moving dislocation is regulated in time by four groupings of dimensionless parameters and for the arrested case by five groupings. This multiplicity presents some problem for representation of the results in the form of type curves. The intractability is somewhat reduced if pressure distributions along the x -axis are only considered. Thus, $y_D = \bar{y}_D$, $z_D = \bar{z}_D = 0$ and $x_D/R_D = \bar{x}_D/\bar{R}_D = \pm 1$ and the number of dimensionless groups controlling the behaviour is reduced by one in both the pre-arrest and post-arrest modes.

3. SPECIALIZATIONS FOR SINGLE BOUNDARIES

Expressions developed for the most general case may be further specialized to represent simple problem geometries in an attempt to understand the interaction of the concurrent mechanisms controlling pressure generation and dissipation. In particular, the two specializations are for a dislocation approaching or leaving a hydraulic boundary.

3.1. Single-boundary approach

Where the dislocation approaches a single boundary, equations (17) and (23) may be modified by completing the summation for $n = 0$ only, and noting that $i = +1$ and $l = +1$ for an impermeable boundary and $l = -1$ for a permeable boundary. The pre-arrest condition may

3.2. Single-boundary departure

A further specialization exists where a dislocation is initiated that moves downwards from an overlying boundary, where the lower hydraulic boundary is infinitely distant, or non-existent. The corresponding equations may be developed from equations (17) and (23), where the summation is restricted to $n = 0$ for the first term and $n = -1$ for the second term. The resulting expressions for the pre-arrest and post-arrest pressure distributions are identical to equations (26) and (28), respectively, where only the magnitude of a_2 differs. For single-boundary departure, a_2 may be specialized as

$$a_2 = 2(b_D - s_D) + U_D t_D \quad (32)$$

where $r(b_D - s_D)$ gives the location below the hydraulic boundary where penetration initiates. For a lower boundary at infinity, the chosen geometry of the system requires that $s_D \rightarrow \infty$ but, regardless, $(b_D - s_D)$ remains finite.

The dimensionless groups controlling behaviour of the system are, for the pre-arrest situation,

$$P_D \bar{R}_D = f \left[U_D R_D; \frac{x_D}{R_D}; \frac{t_D}{R_D^2}; \frac{(b_D - s_D)}{R_D} \right] \quad (33)$$

and for the post-arrest condition,

$$P_D \bar{R}_D = f \left[U_D \bar{R}_D; \frac{\bar{x}_D}{\bar{R}_D}; \frac{(t_D - t'_D)}{\bar{R}_D^2}; \frac{t_D}{\bar{R}_D^2}; \frac{(b_D - s_D)}{\bar{R}_D} \right] \quad (34)$$

Similar to the behaviour of a dislocation approaching a hydraulic boundary, the infinite homogeneous body solution is modified through the second bracketed terms of equations (26) and (28). The significant limiting cases are, for a remote upper bounding layer,

$$(b_D - s_D) \rightarrow \infty \quad \text{and} \quad \exp \left[(2x_D - a_2) \left(\frac{\eta^2 a_2}{R_D^2} - U_D \right) \right] \rightarrow 0 \quad (35)$$

representing insignificant modification of the infinite homogeneous body problem, and where

$$x_D - (b_D - s_D) = \frac{1}{2} U_D t_D \quad \text{and} \quad \exp \left[(2x_D - a_2) \left(\frac{\eta^2 a_2}{R_D^2} - U_D \right) \right] \rightarrow 1 \quad (36)$$

confirming that the boundary conditions at $x = (b - s) - Ut$, corresponding to the upper hydraulic boundary, are correctly and continuously enforced.

4. PORE-PRESSURE GENERATION

The magnitudes of pore pressures generated as a dislocation approaches an underlying hydraulic boundary may be used as an analogue to piezocone penetration in the presence of layering. Since piezocone pressures are normally recorded with depth, it is convenient to restate dimensionless time t_D in terms of a height ($w_D = w/r$) above the interface. Since, from Figure 1, $w = s + x - Ut$,

$$t_D = \frac{2}{U_D} (s_D + x_D - w_D) \quad (37)$$

and the appropriate dimensionless groupings are therefore

$$P_D R_D = f \left(U_D R_D; \frac{x_D}{R_D}; \frac{w_D}{R_D}; \frac{s_D}{R_D}; \frac{b_D}{R_D} \right) \quad (38)$$

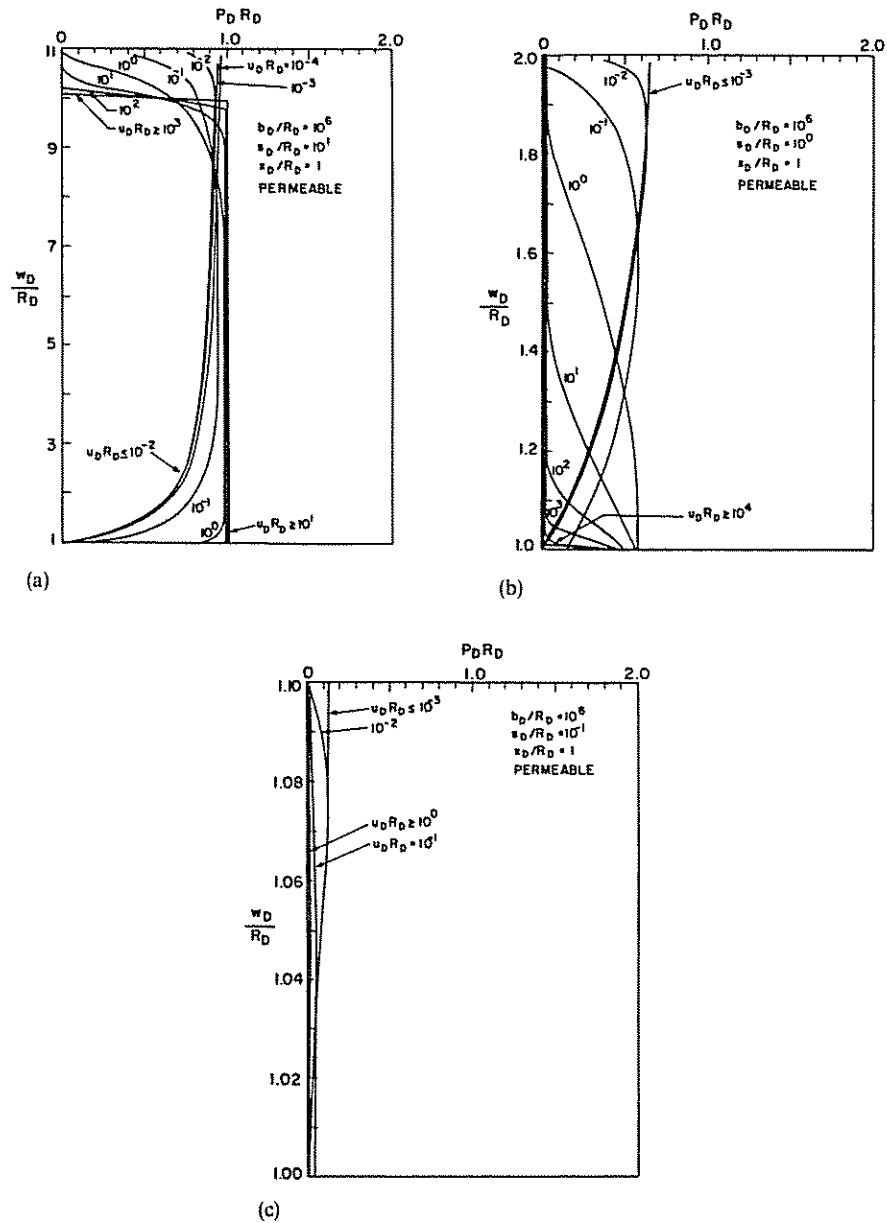


Figure 4. Pressure-generation profiles on the x -axis (shaft) for a dislocation approaching a permeable lower boundary for (a) $s_D/R_D = 10^1$, (b) $s_D/R_D = 10^0$ and (c) $s_D/R_D = 10^{-1}$

boundary. The development of pore pressures are most rapid for small magnitudes of dimensionless penetration rate, corresponding to low penetration velocities or their corollary of high magnitude of consolidation coefficient, c . Little influence of the boundary is seen as it is approached by the dislocation at high rate [$U_D R_D \geq 10^1$ in Figure 3(a)] or conversely, where the coefficient of consolidation is sufficiently low that pressure generation has not yet sufficiently

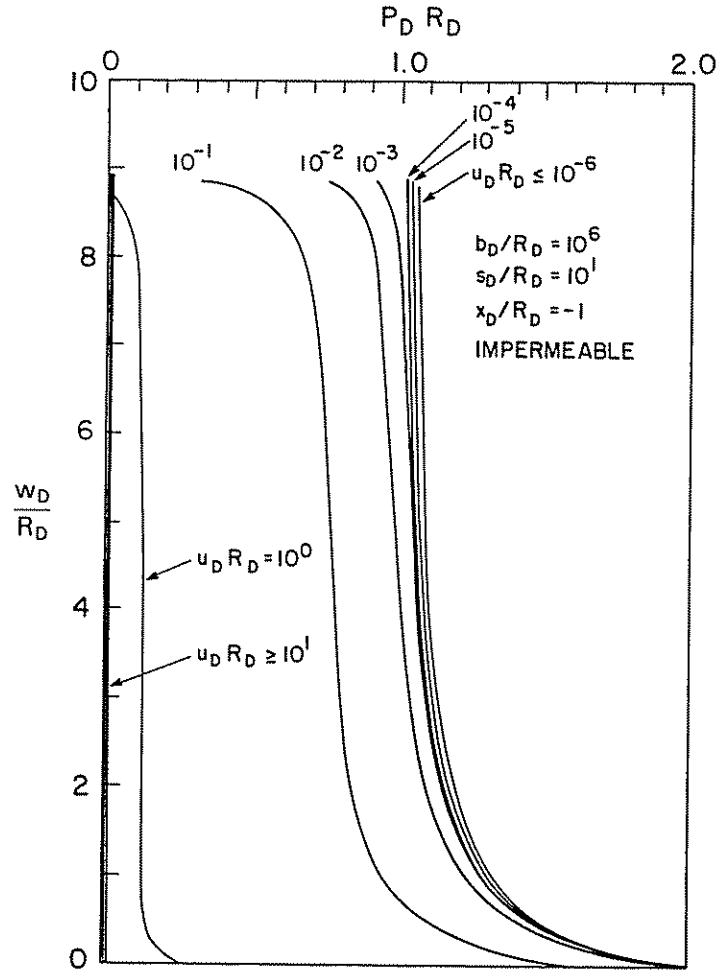
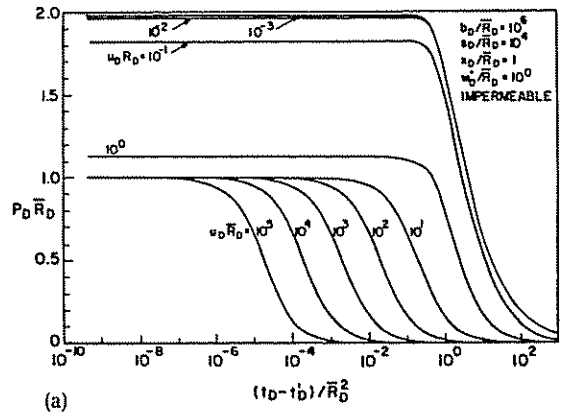


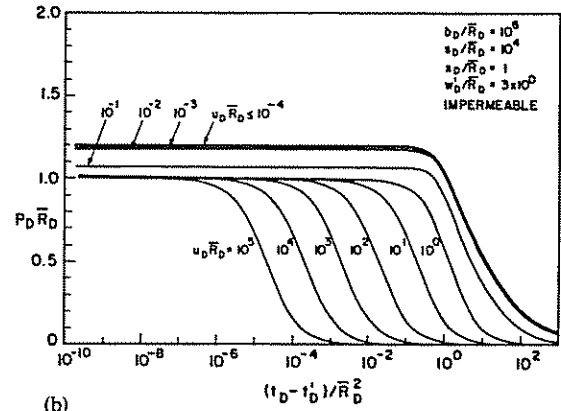
Figure 6. Pressure-generation profiles on the negative x -axis (tip) for a dislocation approaching an impermeable lower boundary for $s_D/R_D = 10^1$

generation is similar for large heights of penetration initiation ($s_D/R_D = 10^1$) but is curtailed as the permeable or constant pressure boundary becomes closer to the start-up location. The pressure response close to the boundary is of opposite sense to that for an impermeable interface with the presence of an interface being felt within the range $w_D/R_D \leq 2$. Again, the greatest influence is apparent for small magnitudes of U_D corresponding to large magnitudes of consolidation coefficient with response being blind to the feature for $U_D R_D \geq 10^1$. Where the depth scales of Figures 4(b) and 4(c) are compressed to a common magnitude in Figures 5(a) and 5(b), the characteristic forms of erratic pore-pressure magnitudes common to piezocone records in layered media are replicated.

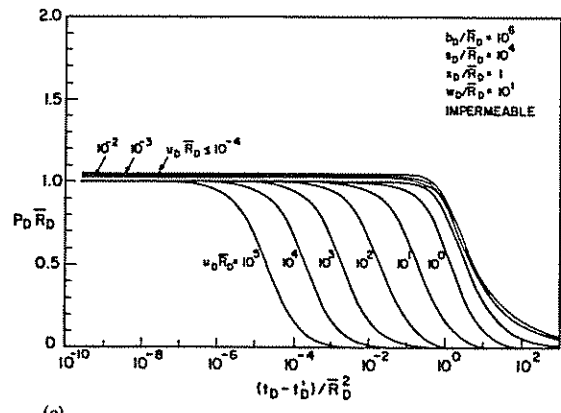
Where the dislocation method is used as an analogue to cone penetration, a centre of volume expansion concept¹³ has been proposed such that the tip for a standard 60 degree cone would be present at $x_D = -0.4082$. Pressure response for a cone approaching an impermeable boundary is illustrated in Figure 6 for $x_D/R_D = -1$ and $s_D/R_D = 10^1$. Only for penetration rate magnitudes



(a)

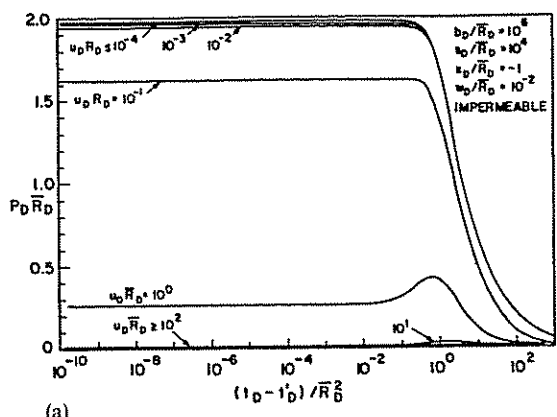


(b)

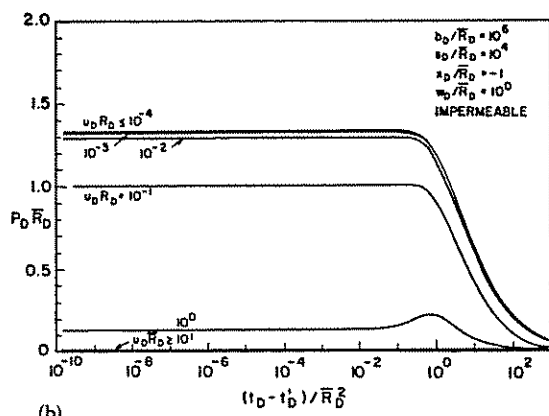


(c)

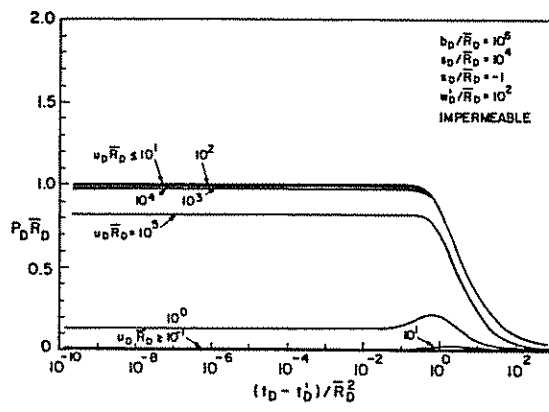
Figure 7. Pressure dissipation on positive x-axis (shaft) close to an impermeable boundary at heights (a) $w'_D/R_D = 10^0$, (b) $w'_D/R_D = 3 \times 10^0$ and (c) $w'_D/R_D = 10^1$



(a)



(b)



(c)

Figure 9. Pressure dissipation on negative x-axis (tip) close to an impermeable boundary at heights (a) $w'_D/R_D = 10^0$, (b) $w'_D/R_D = 3 \times 10^0$ and (c) $w'_D/R_D = 10^1$

3. The prior length of visibility for $U_D R_D \leq 10^0$ is not significantly influenced by the dimensionless penetration rate parameter $U_D R_D$, suggesting an invariance under a broad range of coefficient of consolidation magnitudes. As $U_D R_D$ decreases, the change in pore pressure elicited by the approached boundary becomes increasingly more apparent. The visibility length is of the order $w_D/R_D \leq 2$ suggesting that, for shaft-mounted monitors, the presence of layering is apparent at a separation ahead of the tip equal to the lag of the monitoring location behind the tip. Thus, hydraulic boundaries are theoretically more visible to monitoring locations remote from the tip when pore pressures are dissipation-controlled, as opposed to the tip when pore-pressure generation dominates. This useful artifact is of reduced significance since absolute pressure magnitudes are inversely proportional to lag behind the tip as $P_D \propto 1/R_D$, and hence, instrument sensitivity becomes of concern.
4. A similar detection length $w_D/R_D \leq 2$ applies to the tip as to shaft pressures. For standard penetration, the detection limit is of the order of 1.5 cm ahead of the tip.
5. For arrest close to a hydraulic boundary, pressures generated around the tip are controlled primarily by the material parameters $U_D \bar{R}_D$ and the proximity of the dislocation as measured through w'_D/\bar{R}_D . Initial steady pressure magnitudes conform to those predicted under constant penetration, and dissipation rates are, surprisingly, little influenced by the presence of boundaries. Parameter determination techniques based on dissipation rates remain therefore relatively unprejudiced by the influence of boundaries and allow layer parameters to be correctly determined. Conversely, parameter estimation methods employing peak-pressure magnitudes are subject to the greatest potential risk

ACKNOWLEDGEMENTS

The support of the Waterloo Centre for Groundwater Research, NSERC and the U.S. National Science Foundation is gratefully acknowledged.

NOTATION

a_1, a_2	dimensionless coefficient (equation (18))
b, b_D	thickness of penetrated layer, dimensionless layer thickness
c	coefficient of consolidation
i, j, l, m	indices (± 1) generalizing series expansions for all boundary conditions
k	permeability
n	integer (1, 2) representing particular image source
p, p^s	total fluid pressure, static or initial fluid pressure
P_D	dimensionless fluid pressure
r	radius of penetrometer
R, R_D	radius to point of interest, dimensionless radius to point of interest
R'_{D_i}, R''_{D_i}	dimensionless radius relative to image dislocations pre-arrest, post-arrest
\bar{R}_D	dimensionless radius to point of interest from arrested tip location
S, S_D	height of penetrometer tip above lower boundary, dimensionless height
t, t', t_D	time, time to penetrometer arrest, dimensionless time
U, U_D	Penetration rate or velocity, dimensionless penetration rate
V	dislocation volume
w, w'	height of penetrometer tip above lower boundary, arrested height